High Barrier Nanocomposite Film with Accelerated Biodegradation by Clay Swelling Induced Fragmentation

Renee L. Timmins, Anil Kumar, Maximilian Röhrl, Karel Havlíček, Seema Agarwal,* and Josef Breu*

Conventional biodegradable polymers such as poly(lactic acid) (PLA) are an attractive alternative to replace traditional nondegradable food packaging films which plague the environment. However, PLA has shown to not be degradable in some environmentally relevant conditions, including within the freshwater systems. Additionally, PLA suffers from very poor barrier properties, which could result in food spoilage. Compositing with clay has been used to improve barrier properties according to tortuous path theory. Here a synthetic, large aspect ratio Na-Hectorite is used that may be utterly delaminated in an organic solvent and composited with PLA by modification with 18-crown-6 (18C6Hec), yielding a castable, homogeneous nematic suspension. Upon drying, thermodynamics drive the suspension toward segregation into sublayers of PLA and partially restacked 18C6Hec in situ. This unique self-assembled nanostructure combines the best of two worlds: The aspect ratio remains high and results in a 99.3% reduction in oxygen permeability. Additionally, the film shows surprisingly high resistance to swelling at elevated humidity, but once soaked in water, clay swelling is triggered, which fragments the film and drastically increases the surface area by 2500%. Accelerated degradation is observed under controlled enzymatic conditions and in an environmentally relevant wastewater medium during CO_2 evolution testing.

1. Introduction

Single-use food packaging has become an essential part of our lifestyle, for not only consumer convenience and hygiene but also to prevent food waste as goods are transported globally. However, with 8 million tons of plastic waste entering the ocean each year, an increasing effort is being made to replace those plastics that would persist in the environment when improperly disposed with degradable alternatives.[1–3] After all, mitigating potentially dangerous effects from micro- and nanoplastics in our ecosystem begins with material design and waste management.[4] Poly(lactic acid) (PLA) is a frontrunner for this position due to several favorable properties, including availability and low cost, zero toxicity, high mechanical strength, ease of production, and ability to derive its raw material from renewable (bio-)resources.[5,6] While PLA meets ASTM standards for compost degradation, numerous reports have shown it to have poor degradation in soil, seawater, and freshwater.[7–9] Therefore, PLA offers a limited solution to the accidental release of plastic into our water systems whose plastic litter is disproportionally composed of packaging.[10,11] Nevertheless, PLA is a weak competitor to typical packaging materials in terms of gas barrier properties, which are necessary to prevent spoilage and extend the shelf-life of packaged food.[12]

Various attempts to accelerate PLA degradation include optimizing its microbial environment or by blending it with other more degradable or water-soluble polymers,[13–16] which increases surface area but ultimately worsens mechanical properties.[17–19] The incorporation of clay filler for this purpose stands out for its practicality and effectiveness as such layered silicate nanocomposites can provide additional improvement in the mechanical, barrier, and thermal properties.[20–23] Since natural clays are hydrophilic, modification of the clay surface via ion exchange with alkyl ammonium compounds is necessary to disperse clay into degradable, hydrophobic polyesters. While this helps disaggregation during melt compounding, delamination into single nanosheets of maximized aspect ratio is difficult, if at all possible. For these PLA/clay nanocomposites, an increase in biodegradation rate and reduction of lag time compared to PLA has been observed and is usually attributed to exposure to terminal hydroxylated edge groups.[22,24,25]

In separate reports, clay nanocomposites have also been used to address the poor barrier properties of degradable polymers for food packaging. Silicate platelets act as an impermeable

R. L. Timmins, A. Kumar, M. Röhrl, S. Agarwal, J. Breu
Bavarian Polymer Institute and Department of Chemistry
University of Bayreuth
Bayreuth 95447, Germany
E-mail: agarwal@uni-bayreuth.de; josef.breu@uni-bayreuth.de
K. Havlíček
Institute for Nanomaterials
Advanced Technology and Innovation
Technical University of Liberec
Studentská 2, Liberec 461 17, Czech Republic

The ORCID identification number(s) for the author(s) of this article can be found under https://doi.org/10.1002/mame.202100727

ADVANCED
SCIENCE NEWS
www.advancedsciencenews.com

Macro-
molecular
Materials and Engineering
www.mame-journal.de

barrier to diffusion, creating a tortuous path for gas molecules, including oxygen and water vapor. Previously in our group, synthetic sodium fluorohectorite (NaHec, $[Na_{0.5}]^{inter}[Mg_{2.5}Li_{0.5}]^{oct}$ $[Si_4]^{tet}O_{10}F_2$) clay has been used to create nanocomposite barrier coatings with various polymer matrices.[26–28] NaHec undergoes the rare phenomenon of repulsive osmotic delamination, which is a thermodynamically allowed process, resulting in gentle and quantitative delamination into a nematic liquid crystalline suspension. With an aspect ratio of 20000, rotation even in very dilute suspensions (<1 vol%) is sterically hindered.[29] This huge aspect ratio is preserved upon solvent evaporation, creating such an elongated diffusion pathway that with a 1.4 µm thick glycol chitosan-intercalated NaHec coating, we have shown that the PLA oxygen barrier could outperform polyethylene terephthalate (PET) by a factor of 180 even at 75% relative humidity (RH).[26] However, similar improvements in barrier properties are challenging to achieve for a neat PLA nanocomposite due to the incompatibility of hydrophilic clays and hydrophobic polyesters, which prevents solution blending of PLA with uniform, 1 nm thick clay monolayers. Other compositing methods like melt blending trigger reaggregation or fail to assure quantitative delamination. In a study by Ray et al. where organically modified montmorillonite (OMMT) was combined with PLA via melt extrusion, an enhancement in the degradation rate of the nanocomposite in compost is observed, yet O_2 permeability is hardly improved from 200 mL mm m^{-2} day^{-1} MPa^{-1} (equivalent to 20265 cm^3 µm m^{-2} day^{-1} atm^{-1}) for neat PLA to 177 mL mm m^{-2} day^{-1} MPa^{-1} for PLA nanocomposite. The poor barrier could be attributed to the mediocre anisotropy (and low aspect ratio of 16 for the silicate filler), creating an insufficient tortuous path to gas permeates.[23] Simply dispersing clay via melt blending into PLA to increase surface area and improve degradation without regard for microstructure misses huge potential to synergistically improve barrier properties by orders of magnitude. In our recent work, we showed a balance of high degradability and good barrier properties by preparing a PLA-layered silicate composite in which PLA and layered silicate layers alternate. This was prepared by filtering layered silicate solution through an electrospun PLA porous membrane and hot-pressing several of such layers together.[30] It would be interesting if such macro phase-separated composites could be prepared in a simple way.

Our group also recently published a method which for the first time, extends the rare phenomenon of osmotic delamination within NaHec into organic, aprotic solvents.[31] Previously limited to aqueous suspensions, osmotic delamination of NaHec was obtained spontaneously in various organic solvents, including *N*-methylformamide (NMF) by the simple addition of crown ethers. The complexation of interlayer sodium with, for example, 18-crown-6 (18C6) renders the hectorite (18C6Hec) surface more hydrophobic. This complex enables repulsive osmotic delamination where adjacent clay layers in the nematic liquid crystalline state are separated by distances large enough to be accessible for polyester macromolecules. In this work, NMF is used to create a stable, homogeneous suspension of PLA and osmotically delaminated 18C6Hec to cast films that showed phase-separated morphology by thermodynamically driven segregation into PLA domains and 18C6Hec tactoids in-situ during film preparation. The film shows surprisingly high resistance to swelling at elevated humidity, but clay swelling is triggered once soaked in water, frag-

menting the film and drastically increasing the surface area by 2500%, which might be favorable for degradation once discarded. This unique self-assembled nanostructure showed impressive barrier values competitive with state-of-the-art high-performance packaging films while also biodegrading faster than pure material in wastewater sludge (**Figure 1**). The details of the preparation procedure, structural characterization, and degradation behavior of nanocomposite PLA films are reported in the present work.

2. Results and Discussion

NaHec and 18C6 can simply be dispersed in a PLA/NMF solution, creating a homogenous and nematic phase as evidenced by the presence of a basal series in the small-angle X-ray scattering (SAXS) trace (**Figure 2**a). As expected for nanosheets, q values scale with q^{-2}.[32] Birefringence of the solution was observed under cross-polarized light (Figure 2a: inset), which further confirms long-range order of the liquid-crystal phase. Self-standing nanocomposite films of ≈60 µm thickness were obtained by consecutively casting eight layers of this suspension via slot die coating on top of each other with intermittent drying. The substrate table was set to 60 °C to prevent the precipitation of PLA (7.2 wt% of blend solution), which is only soluble at elevated temperatures. Through the use of slot die coating, precise and uniform wet layers of suspension can be deposited onto a PET substrate from a slotted die head. Slot die coating is an industrially scalable coating method that can be particularly useful in making nanocomposite layers due to the shear-induced alignment of nanosheets within viscous solutions during processing. Resulting nanocomposite layers lack folding or crumbling defects of the nanosheets and instead present a perfect texture with all nanosheets aligned isotopically in the plane of the film.[33] The thickness of the wet layer can be tuned by machine parameters, and the dry layer thickness can be tuned by adjustment of suspension solid content (PLA + clay). Each wet layer is partially dried before the subsequent layer is coated on top, with partial solvation of the previous layer by the wet layer ensuring adhesion. Here, eight layers were deemed an optimal balance of the solution solid content and drying time of each layer.

Upon evaporation of the solvent from the coated 18C6Hec/PLA layer, the confinement of the polymer becomes ever more severe, and the concomitant entropy losses will eventually thermodynamically drive segregation of polymer and 18C6Hec nanosheets. Yet, segregation is severely hindered as mobility becomes increasingly restricted with the formation of the tortuous path. The resulting stratified nanostructure (Figure 2b) contains many randomly alternating PLA domains separating restacked 18C6Hec tactoids (i.e., 1D crystals) generated in-situ via self-assembly. According to transmission electron microscopy (TEM) micrographs (Figure 2c) obtained of the sample cross-sections prepared by cryo-ion-slicing, the segregated 18C6Hec tactoids typically have a thickness of 120 nm. Consequently, a film of 60 µm would be comprised of some 118 tactoids separated by PLA domains of typically 414 nm thickness. The partial reaggregation creates tactoids with an aspect ratio that is reduced by a factor equal to the number of layers in the stack. Since the aspect ratio of a single nanosheet of Hec is as large as 20 000, a stack of 120 clay layers still has an appreciable aspect ratio of 166 without even considering extension in the
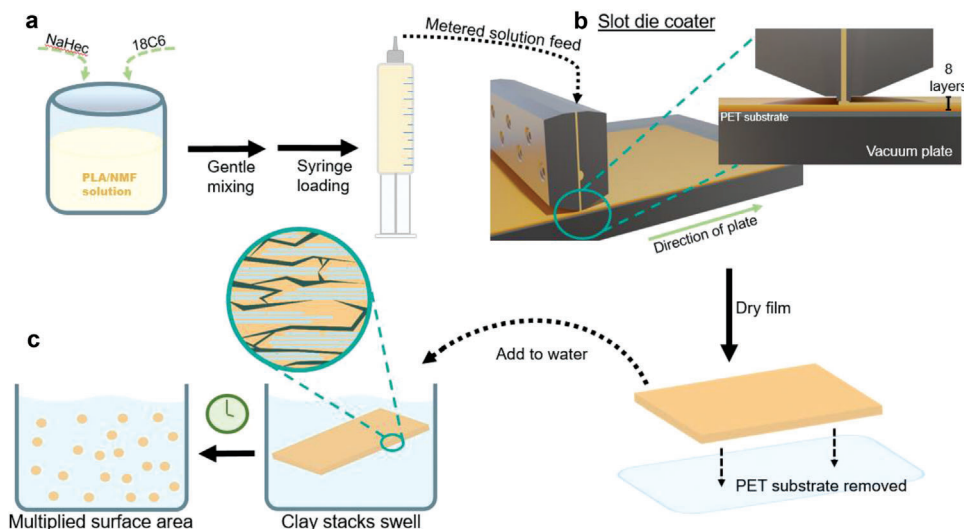
Figure 1. Schematic illustrating fabrication and fragmentation of PLA/18C6Hec films. a) Mixing of NaHec and 18C6 into a PLA/NMF solution. b) Suspension is loaded into a syringe which is then fed into the slot die coater where eight wet layers are coated successively onto a PET substrate. Once the film is dried, the PET substrate is removed. c) When film is immersed into water, clay swelling exerts stress-triggered fragmentation.

width of the tactoids due to the offset stacking of nanosheets (band-like aggregates). This is much larger than the aspect ratio of typical fundamental particles of montmorillonite (10–15). According to Cussler, the barrier improvement factor scales with the square of the aspect ratio.[34] The potential for barrier improvement (ratio of the permeability of the neat polymer film to the permeability of the nanocomposite) is thus expected to nevertheless be immense for the hectorite filler despite partial reaggregation. Using the aspect ratio of 166, a theoretical barrier improvement factor of 97 is expected (Equation S1, Supporting Information).

XRD patterns from the nanocomposite films taken in reflection mode show a 00l series (Figure S1, Supporting Information) with a spacing of 17.7 Å ($2\theta = 4.99°$), indicating that 18C6 remain complexed to the hectorite sheets during film production and that within the hectorite tactoids, there is an absence of PLA. The previously reported d-spacing of a pure 18C6Hec is even larger (18.3 Å),[31] while without a complexed 18C6, NaHec has a d-spacing of 12.5 Å.[35] Although pure NaHec is sensitive to humidity, the complexation by 18C6 reduces hydrophilicity, thus reducing its ability to swell in the presence of water vapor.[31] As water acts as a plasticizer, swelling will increase segment mobility and consequently permeability. Therefore, the moisture sensitivity of 18C6Hec stacks in the PLA nanocomposite was systematically evaluated by monitoring changes in d-spacing as a function of RH (Figure 2d). After equilibration at 90% RH, the d-spacing increased by as little as 8 % relative to dry conditions, indicating minimal swelling of clay layers. Previous studies using unmodified NaHec/polyvinylpyrrolidone (PVP) nanocomposite reported that the d-spacing increased approximately 80% after exposure to the same increase in humidity.[27] This suggests little sensitivity of the PLA/18C6Hec barrier to elevated RH. At 95% RH, however, a steeper increase in d-spacing indicated the onset of more significant layer swelling.

The resistance to swelling at high humidity is indeed reflected practically in the gas barrier properties of the nanocomposite

film. Oxygen transmission rates (OTR) are of prime importance when considering films as a food packaging material. While this value is dependent on film thickness, oxygen permeability (OP) is normalized for film thickness and therefore allows for comparison between different films. OP was measured at 65 % RH, as per the ISO 14663-2 standard (**Figure 3**a). Neat PLA film had an OP of 17775 cm^3 μm m^{-2} day^{-1} atm^{-1}, which was reduced by 99.3 % to 124 cm^3 μm m^{-2} day^{-1} atm^{-1} by compounding with 18C6Hec. This OP outperforms reported values for the common packaging material PET and is even competitive with high-performance poly(vinylidene dichloride) (PVDC).[36] OTRs are reported in Table S1 (Supporting Information). Despite the partial restacking of 18C6Hec, the diffusion path created is nevertheless tortuous due to long, thin band-like clay structures extending along the plane of the film. This particular tactoid morphology creates impermeable walls that extend farther in the direction of the film than would be possible with individual clay sheets. Accordingly, the experimentally observed barrier improvement factor (143) is even higher than theoretical calculations.

Although this film has a tolerance for water vapor, quite surprisingly, it was found to promptly fragment when immersing it into an aqueous solution of proteinase K enzyme for degradation testing. Whenever brought into contact with water, the film disintegrated into small pieces within an hour, multiplying the surface area accessible for degradation (Figure S2, Supporting Information). According to Brunauer–Emmett–Teller (BET) analysis, the surface area of the nanocomposite after sitting in water for 24 h without external forces is 0.372 m^2 g^{-1}, which is more than a 2500% increase from the original surface area of 0.014 m^2 g^{-1}. The surface area has been identified as an important factor for rapid biodegradation of PLA,[37] thus the fragmentation of the PLA/18C6Hec film resulting in a dramatic increase in the surface area could be contributing to its accelerated enzymatic degradation (Figure 3b). After just 5 d, the PLA/18C6Hec film reached complete degradation at approximately 90 % weight loss, con-
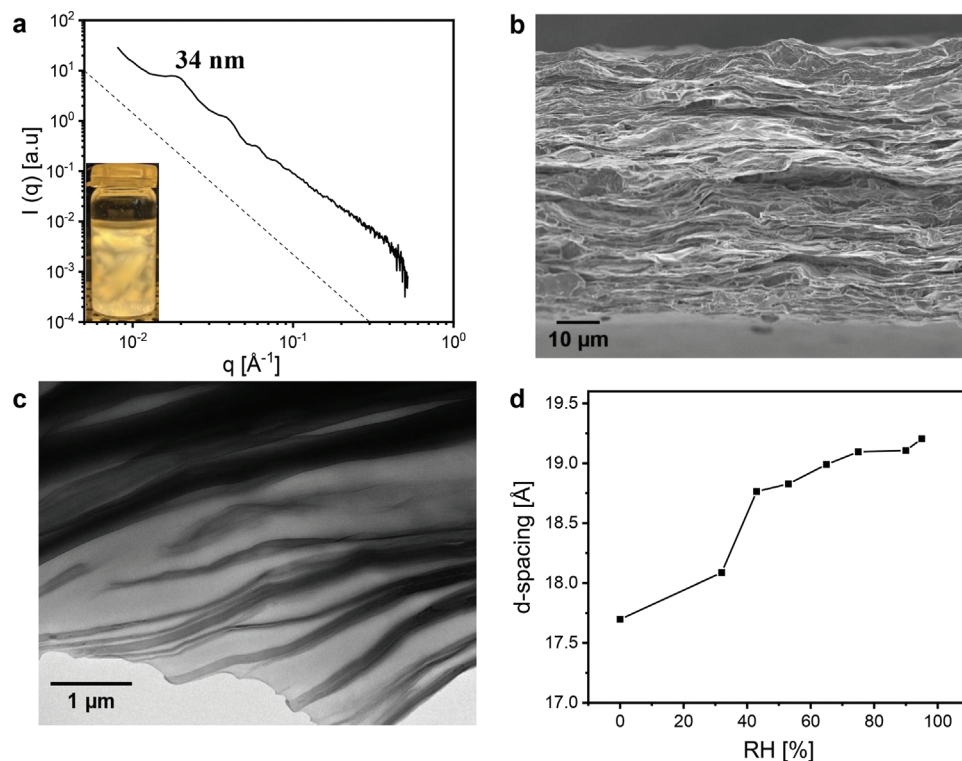
Figure 2. Characterization of nematic suspension and self-standing film. a) 1D SAXS pattern of concentrated PLA/18C6Hec suspension in NMF. Dotted line shows q^{-2} scale. Inset: PLA/18C6Hec suspension in NMF displaying birefringence under cross-polarized light. b) SEM image of PLA/18C6Hec film cross-section. c) TEM image of PLA/18C6Hec film cross-section. d) Swelling behavior of PLA/18C6Hec film observed from d_{001} peaks on XRD traces at an increasing relative humidity.
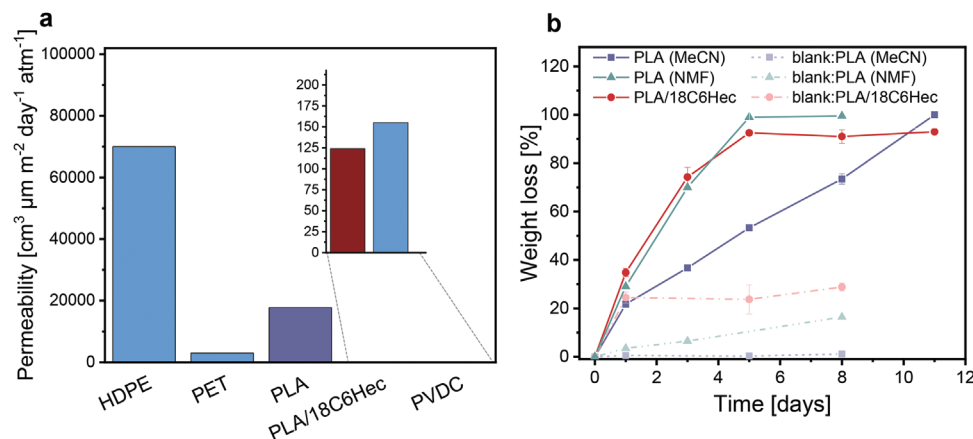

Figure 3. Permeability and degradation studies on PLA/18C6Hec film. a) Oxygen permeability at 65% RH and 23 °C for PLA/18C6 nanocomposite film compared to PLA and other films reported in ref. [31]. b) Weight loss measured from proteinase K enzymatic degradation. Blank trial refers to test conducted using buffer solution without enzyme.* Permeability measured at 50% RH and 23 °C.

sidering 16 wt% of the film is hectorite clay. This is more than twice as fast as the neat PLA film that was cast from acetonitrile (MeCN), which took 11 d to reach complete degradation under similar conditions.

It is important to note that the weight loss curve of the PLA/18C6Hec film is very similar to the weight loss curve of PLA that was cast from NMF. PLA cast from NMF differs from PLA cast from MeCN in two ways. First, PLA cast from NMF

has a significantly reduced molecular weight compared to PLA cast from MeCN. This difference is apparent when comparing the day 0 molecular weight distributions from gel permeation chromatography (GPC) of PLA cast from MeCN and the PLA in the nanocomposite cast from NMF in **Figure 4**. The premature molecular weight shift is attributed to the high-temperature dissolution of PLA into NMF causing chain cleavage. Low initial PLA molecular weight is an additional factor contributing
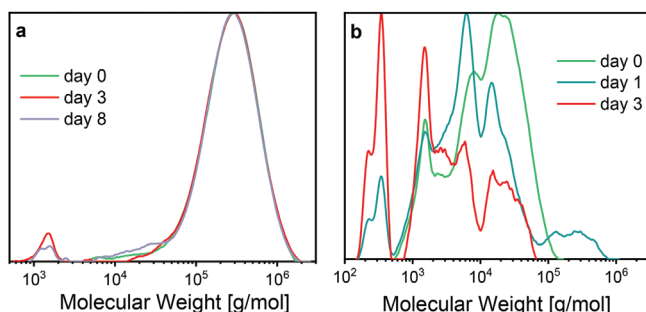
ADVANCED
SCIENCE NEWS
www.advancedsciencenews.com

[M] acro-
olecular
Materials and Engineering
www.mame-journal.de

Figure 4. Gel-permeation chromatography traces of a) PLA (cast from MeCN) and b) PLA/18C6Hec films after enzymatic degradation for different days.

to accelerated degradation, according to the systematic study by Husárová et al.[37] Second, this low molecular weight PLA, as a result of chain cleavage, is very mechanically weak without the hectorite reinforcement and therefore does not form a self-standing film that could be peeled off its PET substrate. The PLA cast from NMF used in the enzymatic degradation test was in the form of small, flakey fragments, i.e., high surface area. Since PLA cast from NMF has both degradation accelerating factors as the PLA/18C6Hec nanocomposite (low initial molecular weight and high surface area), it would be expected that these two materials have a similar degradation rate. The addition of the clay to the low molecular weight PLA provides mechanical support and ability to form a self-standing film without losing the beneficial characteristics for rapid degradation. Due to the extremely poor structural integrity of PLA cast from NMF, a comparison between PLA cast from MeCN, which is much closer to a realistic commercial film, is perhaps more relevant.

The GPC traces of enzymatic degradation samples indicate a surface erosion mechanism of PLA cast from MeCN by showing minimal changes in molecular weight after 8 d (Figure 4). In contrast, we can confirm the further chain cleavage in the PLA/18C6Hec sample by the significant transition to lower molecular weight species appearing after just 3 d, indicating a change in mechanism to bulk degradation for the nanocomposite film. Although the PLA/18C6Hec sample had preexisting molecular weight shifts left, even the highest molecular weight species are nevertheless drastically reduced only after exposure to enzyme solution.

Scanning electron microscopy (SEM) images (**Figure 5**) taken from the PLA (MeCN) and PLA/18C6Hec degradation samples throughout the test show increasing surface roughness of PLA from initial to day 8, corroborating surface erosion as the primary mechanism. Contrary to PLA, the initially smooth surface of the PLA/18C6Hec nanocomposite has fallen apart into thin, open layers of clay and PLA after just 3 d. By day 8, the return of a smooth surface suggests primarily only clay platelets remain.

Degradation of PLA in the nanocomposite is further confirmed by Raman spectroscopy of degraded samples showing the disappearance of the characteristic 1774 cm^{-1} PLA ester peak after 5 d (Figure S3, Supporting Information). Additionally, both differential scanning calorimetry (DSC) scans and ^{1}H NMR could no longer detect the presence of PLA in the nanocomposite

remnants after 5 d as well (Table S2 and Figure S4, Supporting Information).

To follow the degradation of the PLA/18C6Hec films under more environmentally relevant conditions, CO_2 evolution tests were performed with a respirometer according to DIN 14851 in an activated sludge wastewater medium. The kinetics of biodegradation were recorded and compared to a neat PLA film cast from MeCN since this is the more relevant comparison. Cumulative CO_2 production was converted into percent biodegradation (**Figure 6**a). The PLA film showed minimal biodegradation (0.4%) at the end of the 45 d, while the PLA/18C6Hec nanocomposite film had significantly accelerated biodegradation (15%). Measuring only the 18C6, added as molecular complexing ligand, revealed that approximately 4% of it is biodegraded within the testing period, dismissing the possibility that this species is responsible for most of the CO_2 release. After the initial phase of strongly accelerated biodegradation for the nanocomposite sample, the biodegradation continues after day 15 at a constant rate of 0.09 % biodegradation per day, which is more than the total PLA biodegradation rate in 45 d. The slowed rate of biodegradation for the nanocomposite may be due to increased crystalline fractions present after the initial rapid consumption of amorphous regions (Table S3, Supporting Information). At the end of the testing period, all that was left of the PLA/18C6Hec film was tiny fragments, while the PLA film remained visually unchanged (Figure 6b). The fragmentation, moreover, prevented any lag phase, as would typically be observed in the biodegradation of PLA and PLA nanocomposites.[38] GPC traces of the PLA sample (Figure S5, Supporting Information) show little change in molecular weight distribution postdegradation testing. Whereas significant shifts to lower molecular weights were observed postdegradation testing for the PLA/18C6Hec film, demonstrating that our nanocomposite film not only fragments in aqueous mediums but also undergoes molecular chain cleavage and accelerated biodegradation. Similar to the enzymatic degradation testing, neat PLA degrades through surface erosion, whereas the nanocomposite film undergoes a bulk biodegradation mechanism facilitated by increased surface area from the fragmentation of the film. These results were repeatable when using wastewater from treatment plants in Bayreuth, Germany, or Liberec, Czech Republic.

Mechanical testing reveals that the PLA/18C6Hec film unfortunately suffers from embrittlement due to the use of low molecular weight PLA and the incorporation of platy clay filler (Table S4, Supporting Information), as is commonly observed in similar systems.[39–41] The elastic modulus of the nanocomposite is comparable to the pure PLA (1.14 and 1.43 GPa, respectively) however the elongation at break is significantly decreased from 9.7% for pure PLLA to 3.5% for PLA/18C6Hec. Such a decrease in elongation is to be expected from an unplasticized nanocomposite containing high filler content (16 wt%). The improvement of the mechanical properties through the use of additives or blending will be the subject of future investigations.

3. Conclusion

In summary, our nanocomposite film addressed two major challenges facing the development of high-performance degradable polymers films: improvement of barrier properties to levels
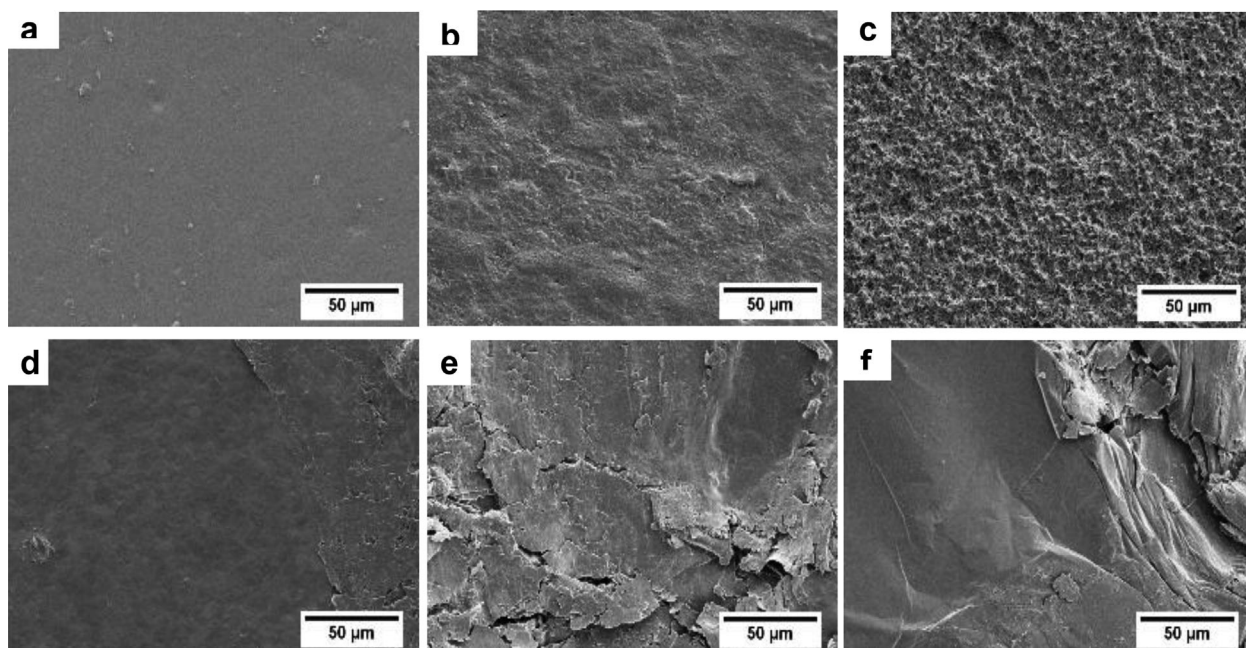
Figure 5. SEM images of films in enzymatic degradation test a–c) for PLA. a) Day 0 (initial), b) day 3, c) day 8. And d–f) for PLA/18C6Hec. d) Day 0 (initial), e) day 3, f) day 8.
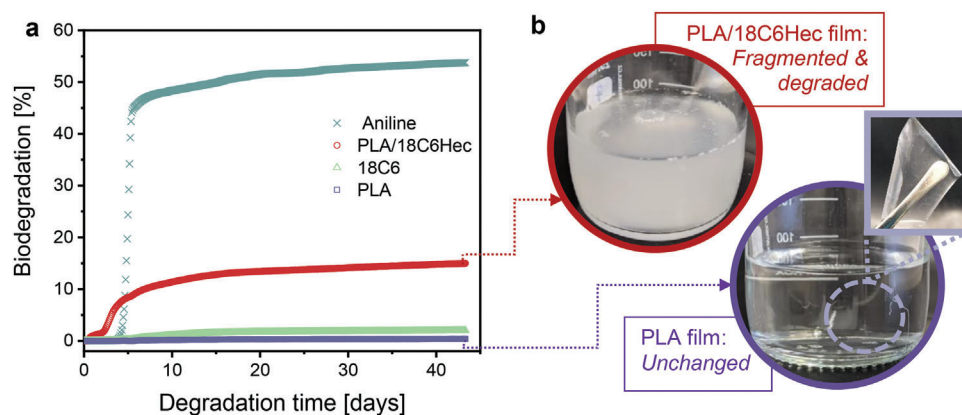

Figure 6. a) Percent biodegradation determined from CO_2 production for degradation of PLA/18C6Hec, 18C6, and PLA (cast from MeCN) in activated sludge medium. Aniline is used as a positive standard. b) Pictures of PLA/18C6Hec and PLA films at the end of degradation testing in activated sludge.

competitive with high-performance materials and enhancement of the ability of PLA to degrade rapidly in wastewater. The water-triggered fragmentation due to the swelling of clay tactoids within the film presents a practical way to optimize the design of current degradable polymers to better suit commercial needs. Although the mechanical properties of this film are not strong enough for practical use as a self-standing material, it is instead highly promising for use as a biodegradable barrier coating. Also, the future work will include the extension of the method presented here into other degradable polymers, conducting degradation testing in different environmentally relevant mediums such as compost, and the avoidance of 18C6.

4. Experimental Section

Material: Sodium fluorohectorite $[Na_{0.5}]^{inter}[Mg_{2.5}Li_{0.5}]^{oct}[Si_4]^{tet}O_{10}F_2$ (Hec) was prepared by employing a synthesis procedure from the melt, as previously reported in the literature.[42] The material features a cation exchange capacity of 1.27 mmol g^{-1}. Ingeo 4043D from Natureworks was used as poly(lactic acid) (PLA). 18-crown-6 (18C6) was provided by abcr with 99% purity. N-methylformamide (NMF, 99%, Alfa Aesar) and acetonitrile (MeCN, 99%, Alfa Aesar) were used as solvent. All reagents were used as received. The polyethylene terephthalate (PET) substrate (36 µm) was purchased from Bleher Folientechnik GmbH (Germany).

Film Fabrication: 5.2 g of PLA was dissolved in NMF (64 g) at 100 °C in a covered round bottom flask until a clear solution was reached. Once the PLA solution was cooled to 50 °C, 1.3 g of each NaHec and 18C6 was

added and mixed for at least one week at room temperature to ensure complete homogenization. Prior to coating, the solution was heated to 60 °C to reduce viscosity during syringe pump loading.

Films were prepared using a TSE Table Coater with a 1-Layer Slot Die 300 mm, AAA (TSE Troller AG, Switzerland). The coating width and wet layer thickness were set to 0.21 m and 88 µm, respectively. The pump flow rate (1.5 mL min^{-1}) and the table speed (0.08 m min^{-1}) were adjusted accordingly. The table temperature was set to 60 °C. A PET foil was used as the base substrate onto which nanocomposite layers would be deposited. The coating gap was set to 168 µm (36 µm PET + 1.5 × 88 µm coating height). After each layer, the foil was left to dry for 45 min, and the coating height was increased by 10 µm. Once eight layers were deposited, the foil was transferred to a vacuum oven at 70 °C and 10^{-3} bar. After the removal of the remaining NMF, the PLA nanocomposite film was carefully peeled off the PET substrate.

For the PLA film sample cast from acetonitrile, PLA was dissolved in acetonitrile (10 wt%) at 60 °C until a clear solution was obtained. For the PLA film sample cast from NMF, PLA was dissolved in NMF (10 wt%) at 100 °C until a clear solution was obtained. Once cooled to room temperature, 18C6 was added (2 wt%) to the solution and mixed overnight. A self-standing film was produced from both of these solutions in the same manner as reported for the PLA nanocomposite, then dried for 4 d at 70 °C.

Enzymatic Degradation: Film samples with (approximately 2 cm x 1 cm) a weight of 40 mg were placed in a glass vial with 5 mL of 0.05 M Tris buffer solution (pH = 8.6) containing 0.2 mg mL^{-1} of Proteinase K (GeneON, Germany) and 0.2 mg mL^{-1} of sodium azide, as per a previously reported method.[43] The vials were then placed in incubation at 37 °C. The buffer/enzyme system was changed every 24 h to retain enzymatic activity. This was done by centrifugation of the solution and removing clear supernatant. Three samples for each experiment were taken at each time interval and were washed with distilled water three times. Collected samples were vacuum dried at room temperature for one week before being subjected to analysis. Control for each film was performed in the same medium without an enzyme.

CO$_2$ Evolution Degradation Testing: DIN 14851:2019 was referred to for carrying out the biodegradation test using activated sludge, after the end of the nitrification process as obtained from the wastewater treatment plant at Bayreuth, Germany. Approximately 75 mg of the film was added to 95 mL of standard medium and 5 mL of supernatant from activated sludge. Aniline was used as the positive sample. The mixture was dosed into 250 mL test bottle, and testing immediately began. The testing period was 45 d. Activated sludge (without any organic substrate) in the same concentration was used as a control. The Micro-Oxymax respirometer equipped with a paramagnetic oxygen sensor and infra-red CO$_2$ sensor (Columbus Instruments International, USA) was used for the measurements.

Characterization: Small-Angle X-Ray Scattering (SAXS): The small-angle X-ray "Ganesha AIR" (SAXSLAB, Denmark) equipment was used to record SAXS patterns. It is equipped with a rotating anode X-ray source (copper, MicoMax 007HF, Rigaku Corporation, Japan). The data was recorded by a position-sensitive detector (PILATUS 300K, Dectris). To cover the range of scattering vectors between 0.006 and 0.5 Å^{-1}, different detector positions were used. Prior to the measurements, the PLA/Hec/18C6 suspension was centrifuged for 1 h (10 000 rpm) to obtain a gel to enhance sensitivity. The measurement of the suspension was performed in 1 mm glass capillaries (Hilgenberg, Germany) at room temperature.

Characterization: Scanning Electron Microscopy (SEM): SEM images of the cross-section of the film were observed using a ZEISS LEO 1530 (Carl Zeiss AG, Germany) operating at 3 kV.

Characterization: Transmission Electron Microscopy (TEM): The PLA/Hec/18C6 nanocomposite film was thinly cut with an Ion Slicer EM-09100IS (JEOL GmbH, Germany). TEM images were then recorded with a JEM-2200FS (JEOL GmbH, Germany) microscope.

Characterization: X-Ray Diffraction (XRD): XRD patterns of the films were recorded using nickel filtered Cu-Kα radiation (λ = 1.54187 Å) in Bragg-Brentano-geometry on an Empyrean diffractometer (PANalytical B.V., the Netherlands) equipped with a Pixel detector. Prior to measure-

ment at 0% RH, a film sample was dried at 70 °C for one week in a vacuum oven (10^{-3} bar). For the measurements at varying RH, samples were equilibrated for at least one week either above a concentrated salt solution (MgCl$_2$ 6H$_2$O (32% RH), K$_2$CO$_3$ (43% RH), Mg(NO$_3$)$_2$ (53% RH)) or in a Memmert HCP105 humidity chamber (Memmert GmBH + Co. KG, Germany) at 25 °C (65, 75, 90, and 95% RH).

Characterization: Oxygen Transmission Rates (OTR): OTRs were determined on a Mocon OX-TRAN 2/21 system (Mocon Inc., USA) with a lower detection limit of 0.05 cm^3 m^{-2} day^{-1} atm^{-1}. The measurements were performed at 23 °C and 65 % RH. A mixture of 98% nitrogen and 2% hydrogen was used as the carrier gas and pure oxygen as permeant (>99.95 %, Linde Sauerstoff 3.5). Film thickness was 59 µm determined using a high-accuracy Digimatic micrometer (Mitutoyo, Japan) with a measuring range of 0–25 mm and a resolution of 0.0001 mm.

Characterization: Brunauer–Emmet–Teller Surface Area Analysis (BET): The surface area was measured with a Quantachrome Autosorb-1 using Kr as the adsorbate at 70 °K. The isotherm was evaluated using the BET method.

Characterization: Gel Permeation Chromatography (GPC): GPC traces were obtained using chloroform as the eluent at a flow rate of 0.5 mL min^{-1} at room temperature. A precolumn PSS SDV (particle size 5 µm) and a column PSS SDV XL linear (particle size 5 µm) calibrated against polystyrene standards (PSS) were used with a PSS SECcurity RI detector. The GPC data was analyzed by the software PSS WinGPC Unity, Build 1321.

Characterization: Raman Spectroscopy: Raman spectra were obtained with the WITec alpha 300 RA+ (Germany) system using a 532 nm laser line and 50 scans. The laser was focused using the maximum 10X magnification objective of the Raman microscope.

Characterization: ^{1}H NMR: NMR spectra were recorded on a Bruker Avance 300 NMR system operating at 300 MHz frequency at room temperature using deuterated chloroform (CDCl$_3$) as a solvent. Chemical shifts (δ) are indicated in parts per million (ppm) with respect to residual solvent signals.

Characterization: Differential Scanning Calorimetry (DSC): DSC scans were obtained with a DSC 204 F1 Phoenix system (Netzsch) with a heating rate of 10 K min^{-1} under an N$_2$ atmosphere. The first heating cycle is used for the determination of melting peaks (T_m), and the second heating cycle is used for the determination of glass transition (T_g).

Characterization: Mechanical Testing: Stress–strain tests were performed with a tensile instrument (Zwick/Roell, BT1-FR0.5TN.D14). The samples for the tensile measurement were cut to the size of 3 mm × 30 mm for a pristine effective tensile length of 10 mm. The test was performed with crosshead speed 5 mm min^{-1} at room temperature for at least ten measurements. The slope of the linear region of the stress-strain curves was used to determine the elasticity modulus.

Supporting Information

Supporting Information is available from the Wiley Online Library or from the author.

Acknowledgements

Conflict of Interest

The authors declare no conflict of interest.

Data Availability Statement

The data that supports the findings of this study are available in the Supporting Information of this article.

Keywords

[1] E. Macarthur, *Science* **2017**, *358*, 843.
[2] S. Agarwal, *Macromol. Chem. Phys.* **2020**, *221*, 2000017.
[3] J. M. Millican, S. Agarwal, *Macromolecules* **2021**, *54*, 4455.
[4] D. M. Mitrano, P. Wick, B. Nowack, *Nat. Nanotechnol.* **2021**, *16*, 491.
[5] M. Karamanlioglu, R. Preziosi, G. D. Robson, *Polym. Degrad. Stab.* **2017**, *137*, 122.
[6] S. Singha, M. S. Hedenqvist, *Polymers* **2020**, 12, 1095.
[7] A. R. Bagheri, C. Laforsch, A. Greiner, S. Agarwal, *Global Challenges* **2017**, *1*, 1700048.
[8] H. Tsuji, K. Suzuyoshi, *Polym. Degrad. Stab.* **2002**, *75*, 347.
[9] H. Tsuji, K. Suzuyoshi, *Polym. Degrad. Stab.* **2002**, *75*, 357.
[10] A. E. Schwarz, T. N. Ligthart, E. Boukris, T. Van Harmelen, *Mar. Pollut. Bull.* **2019**, *143*, 92.
[11] C. J. Moore, *Environ. Res.* **2008**, *108*, 131.
[12] M. Zabihzadeh Khajavi, A. Ebrahimi, M. Yousefi, S. Ahmadi, M. Farhoodi, A. Mirza Alizadeh, M. Taslikh, *Food Eng. Rev.* **2020**, *12*, 346.
[13] S. Sukkhum, *J. Microbiol. Biotechnol.* **2012**, *22*, 92.
[14] Y. Tokiwa, M. Konno, H. Nishida, *Chem. Lett.* **1999**, *28*, 355.
[15] Y. Oda, A. Yonetsu, T. Urakami, K. Tonomura, *J. Polym. Environ.* **2000**, *8*, 29.
[16] A. Kumar, A. R. Weig, S. Agarwal, *Macromol. Mater. Eng.* **2021**, 2100602. https://doi.org/10.1002/mame.202100602.
[17] C. Vasile, D. Pamfil, M. Râpă, R. N. Darie-Niţă, A. C. Mitelut, E. E. Popa, P. A. Popescu, M. C. Draghici, M. E. Popa, *Composites, Part B* **2018**, *142*, 251.
[18] S. Dharmalingam, D. G. Hayes, L. C. Wadsworth, R. N. Dunlap, J. M. Debruyn, J. Lee, A. L. Wszelaki, *J. Polym. Environ.* **2015**, *23*, 302.
[19] W. Y. Jang, B. Y. Shin, T. J. Lee, R. Narayan, *J. Ind. Eng. Chem.* **2007**, *13*, 457.
[20] J. K. Pandey, K. Raghunatha Reddy, A. Pratheep Kumar, R. P. Singh, *Polym. Degrad. Stab.* **2005**, *88*, 234.
[21] H. C. Koh, J.i S. Park, M.i A.e Jeong, H. Y. Hwang, Y. T. Hong, S. Y. Ha, S. Y. Nam, *Desalination* **2008**, *233*, 201.
[22] K. Fukushima, C. Abbate, D. Tabuani, M. Gennari, G. Camino, *Polym. Degrad. Stab.* **2009**, *94*, 1646.
[23] S. Sinha Ray, K. Yamada, M. Okamoto, K. Ueda, *Nano Lett.* **2002**, *2*, 1093.
[24] E. Castro-Aguirre, R. Auras, S. Selke, M. Rubino, T. Marsh, *Polymers* **2018**, 10, 202.
[25] S. Sinha Ray, M. Okamoto, *Macromol. Mater. Eng.* **2003**, *288*, 936.
[26] C. Habel, M. Schöttle, M. Daab, N. J. Eichstaedt, D. Wagner, H. Bakhshi, S. Agarwal, M. A. Horn, J. Breu, *Macromol. Mater. Eng.* **2018**, *303*, 1800333.
[27] T. Schilling, C. Habel, S. Rosenfeldt, M. Röhrl, J. Breu, *ACS Appl. Polym. Mater.* **2020**, *2*, 3010.
[28] C. Habel, E. S. Tsurko, R. L. Timmins, J. Hutschreuther, R. Kunz, D. D. Schuchardt, S. Rosenfeldt, V. Altstädt, J. Breu, *ACS Nano* **2020**, *14*, 7018.
[29] S. Rosenfeldt, M. Stöter, M. Schlenk, T. Martin, R. Q. Albuquerque, S. Förster, J. Breu, *Langmuir* **2016**, *32*, 10582.
[30] J. Zhu, C. Habel, T. Schilling, A. Greiner, J. Breu, S. Agarwal, *Macromol. Mater. Eng.* **2019**, *304*, 1800779.
[31] V. Dudko, K. Ottermann, S. Rosenfeldt, G. Papastavrou, J. Breu, *Langmuir* **2021**, *37*, 461.
[32] L. Boldon, F. Laliberte, L. Liu, *Nano Rev.* **2015**, *6*, 25661.
[33] M. Röhrl, J. H. Mettke, S. Rosenfeldt, H. Schmalz, U. Mansfeld, R. L. Timmins, C. Habel, J. Breu, F. Durst, *J. Coat. Technol. Res.* **2021**, 1. https://doi.org/10.1007/s11998-021-00535-4.
[34] E. L. Cussler, S. E. Hughes, W. J. Ward, R. Aris, *J. Membr. Sci.* **1988**, *38*, 161.
[35] H. Kalo, W. Milius, J. Breu, *RSC Adv.* **2012**, *2*, 8452.
[36] C. Maes, W. Luyten, G. Herremans, R. Peeters, R. Carleer, M. Buntinx, *Polym. Rev.* **2018**, *58*, 209.
[37] L. Husárová, S. Pekařová, P. Stloukal, P. Kucharzcyk, V. Verney, S. Commereuc, A. Ramone, M. Koutny, *Int. J. Biol. Macromol.* **2014**, *71*, 155.
[38] P. Stloukal, S. Pekařová, A. Kalendova, H. Mattausch, S. Laske, C. Holzer, L. Chitu, S. Bodner, G. Maier, M. Slouf, M. Koutny, *Waste Manage.* **2015**, *42*, 31.
[39] A. B. Gomez-Gamez, A. Yebra-Rodriguez, A. Peñas-Sanjuan, B. Soriano-Cuadrado, J. Jimenez-Millan, *Appl. Clay Sci.* **2020**, *198*, 105818.
[40] Y. Guo, K. Yang, X. Zuo, Y. Xue, C. Marmorat, Y. Liu, C. -. C. Chang, M. H. Rafailovich, *Polymer* **2016**, *83*, 246.
[41] P. Russo, S. Cammarano, E. Bilotti, T. Peijs, P. Cerruti, D. Acierno, *J. Appl. Polym. Sci.* **2014**, *131*, 39798.
[42] H. Kalo, M. W. Möller, M. Ziadeh, D. Dolejš, J. Breu, *Appl. Clay Sci.* **2010**, *48*, 39.
[43] S. Li, A. Girard, H. Garreau, M. Vert, *Polym. Degrad. Stab.* **2000**, *71*, 61.